BIOCHEMISTRY

# Enhancing HIV-1 latency reversal through regulating the elongating RNA Pol II pause-release by a small-molecule disruptor of PAF1C

**Shimaa H. A. Soliman[1], William J. Cisneros[2,3], Marta Iwanaszko[1], Yuki Aoi[1], Sheetal Ganesan[1], Miriam Walter[2], Jacob M. Zeidner[1], Rama K. Mishra[1], Eun-Young Kim[2], Steven M. Wolinsky[2], Judd F. Hultquist[2,3], Ali Shilatifard[1]***



**The polymerase-associated factor 1 complex (PAF1C) is a key, post-initiation transcriptional regulator of both promoter-proximal pausing and productive elongation catalyzed by RNA Pol II and is also involved in transcriptional repression of viral gene expression during human immunodeficiency virus–1 (HIV-1) latency. Using a molecular docking–based compound screen in silico and global sequencing–based candidate evaluation in vivo, we identified a first-in-class, small-molecule inhibitor of PAF1C (iPAF1C) that disrupts PAF1 chromatin occupancy and induces global release of promoter-proximal paused RNA Pol II into gene bodies. Transcriptomic analysis revealed that iPAF1C treatment mimics acute PAF1 subunit depletion and impairs RNA Pol II pausing at heat shock–down-regulated genes. Furthermore, iPAF1C enhances the activity of diverse HIV-1 latency reversal agents both in cell line latency models and in primary cells from persons living with HIV-1. In sum, this study demonstrates that efficient disruption of PAF1C by a first-in-class, small-molecule inhibitor may have therapeutic potential for improving current HIV-1 latency reversal strategies.**

## INTRODUCTION

The complex regulatory processes governing gene expression require the concerted action of many transcriptional regulators (*1*, *2*). Transcription starts with formation of the preinitiation complex containing RNA polymerase II (RNA Pol II) and associated general transcription factors (*3*, *4*). RNA Pol II escapes the promoter regions upon phosphorylation of serine-5 in its C-terminal domain (CTD) by cyclin-dependent kinase 7 (CDK7) (*5*–*7*). Serine-5–phosphorylated Pol II initiates transcription at the transcription start site (TSS) and proceeds ~20 to 60 nucleotides downstream before pausing, during which it remains transcriptionally engaged and stably associated with nascent transcripts (*8*). The transition from the paused state into productive elongation is regulated by several negative elongation factors and by positive transcription elongation factor-b (P-TEFb), composed of cyclin T1 (CCNT1) and CDK9, which phosphorylates the RNA Pol II CTD at serine-2 (*9*–*11*). Dysregulation of RNA Pol II pause-release is associated with disease states and plays a critical role in the transcription and latency of viruses including herpes simplex virus 1 (HSV1) and human immunodeficiency virus–1 (HIV-1) (*12*, *13*). Therapeutic targeting of this crucial process requires better mechanistic understanding for which the development of unidentified small molecules to modulate RNA Pol II pausing factors is an essential step.

The polymerase-associated factor 1 complex (PAF1C) was initially identified as a protein complex copurified with yeast RNA Pol II (*14*). PAF1C is evolutionary conserved from yeast to humans and consists of five conserved subunits—PAF1, LEO1, CTR9, RTF1, and CDC73—as well as a mammalian-specific subunit, SKI8 (*15*–*18*). PAF1C plays several critical roles in regulating transcription and epigenetic chromatin modification. For example, PAF1C mediates mono-ubiquitination of histone H2B on lysine-123 in yeast (lysine-120 in humans) through its interaction with Rad6 to regulate a myriad of processes including DNA repair, cell cycle regulation, and autophagy (*19*–*24*). The crystal and cryo–electron microcopy (cryo-EM) structures of PAF1C have been solved, and several structural studies have revealed that formation of the CTR9/PAF1 subcomplex is indispensable for full PAF1C assembly (*17*, *25*–*29*).

PAF1C both positively and negatively regulates transcriptional elongation (*1*, *30*–*33*). We recently demonstrated that PAF1 is recruited by SPT6 to maintain RNA Pol II in a paused state at promoter-proximal regions (*34*). Depletion of PAF1 results in increased recruitment of the P-TEFb–containing super elongation complex (SEC), which increases RNA Pol II release into gene bodies (*30*). Likewise, at MYC-dependent loci, PAF1C associates with MYC to inhibit histone acetylation and the recruitment of P-TEFb to RNA Pol II, resulting in paused polymerase and transcription inhibition (*35*). However, while PAF1C inhibits the licensing of transcriptional elongation at many loci, it also plays a positive role in the progression of productive transcriptional elongation by enhancing RNA Pol II rate and processivity. Depletion of PAF1 reduces elongation rates, resulting in premature termination and decreased transcript abundance, especially for long genes (*34*).

Promoter-proximal pausing also regulates integrated HIV-1 proviruses, which can evade this regulation via direct recruitment of P-TEFb to nascent viral transcription sites by the viral protein Tat (*36*–*38*). PAF1C participates in the regulation of RNA Pol II pausing at the HIV-1 long terminal repeat (LTR) promoter, and its depletion results in an increase in HIV-1 transcription (*39*).

[1]Simpson Querrey Institute for Epigenetics, Department of Biochemistry and Molecular Genetics Feinberg School of Medicine, Northwestern University, Chicago, IL 60611, USA. [2]Division of Infectious Diseases, Department of Medicine, Feinberg School of Medicine, Northwestern University, Chicago, IL 60611, USA. [3]Center for Pathogen Genomics and Microbial Evolution, Havey Institute for Global Health, Feinberg School of Medicine, Northwestern University, Chicago, IL 60611, USA.
*Corresponding author. Email: ash@northwestern.edu

Therefore, PAF1C is implicated in the regulation of HIV-1 latency, a major and persistent obstacle to the development of a functional cure (*40*–*42*). Most of the latent HIV-1 reservoir is thought to be composed of long-lived, memory $CD4^+$ T cells that contain transcriptionally inhibited, replication-competent HIV-1 proviruses (*43*, *44*). Multiple blocks to viral transcription have been described to play a role in HIV-1 latency establishment and maintenance, including several blocks to transcriptional elongation.

One of the earliest strategies designed to deplete the latent HIV-1 reservoir, referred to as "shock and kill," posited that latency-reversing agents (LRAs) could induce viral expression in latently infected cells to activate viral clearance (*45*, *46*). Several LRAs have since been described, including T cell stimulatory agents, kinase activators, and chromatin modifiers (*47*–*50*). While effective at reactivating latent proviruses ex vivo, these regimens proved therapeutically untenable, because they demonstrated remarkable variability in their reactivation potential on both a cell-to-cell and provirus-by-provirus basis (*41*, *51*). These studies emphasized that HIV latency is mediated through multiple layers of transcriptional blockade, all of which must be overcome to induce latency reversal. Therefore, further study not only of HIV latency but also of transcriptional regulation as a whole necessitates the development of yet unidentified LRAs as molecular probes.

In this study, we investigated the therapeutic potential of PAF1C targeting using previously unidentified small molecular inhibitor that targets the PAF1 interaction groove of CTR9 to disrupt complex integrity. By performing molecular docking simulations, we virtually screened over 10 million compounds from the ZINC database and identified 30 lead candidates (*52*). From these, we identified a bona fide small molecular inhibitor named iPAF1C that impairs PAF1 chromatin localization and induces release of RNA Pol II into gene bodies at most loci. Global transcriptome analysis revealed that iPAF1C treatment mimics the effects of acute PAF1 depletion on both nascent and mature transcripts. The inhibitor was similarly able to relieve promoter-proximal pausing after heat shock (HS), a well-characterized stimulus that regulates transcriptional elongation. The therapeutic application of iPAF1C to HIV was examined using both cell line for HIV latency models and ex vivo cells from virally suppressed HIV patients. Notably, iPAF1C enhanced the reactivation potential of diverse LRAs in both systems and was also singly sufficient for reactivation of latent proviruses in patient cells. In sum, this study identifies and validates a first-in-class, small-molecule iPAF1C, a critical tool for understanding the role of PAF1C in transcriptional control and in diverse disease states.

## RESULTS

### Structure-based compound screening was used to identify potential small-molecule inhibitors of PAF1C

Prior structural and biochemical studies demonstrated that full assembly of the six-subunit PAF1C is nucleated by subcomplex formation between the subunits PAF1 and CTR9, which interact via a conserved CTR9 binding groove (*25*, *26*, *29*). Therefore, we sought to identify a small-molecule inhibitor that could bind to this pocket and disrupt PAF1 binding to the CTR9 groove. Therefore, we performed in silico, structure-based [Protein Data Bank (PDB): 5ZYQ] molecular docking simulations for 10 million small molecules available at the ZINC database (*52*), identifying 30 candidates with strong predicted values for disruption in this pocket (Fig. 1A).

We had previously demonstrated a central role for PAF1C in transcriptional pausing by RNA Pol II, and we reasoned that a bona fide small molecular disruptor of PAF1-CTR9 interaction should also induce the release of RNA Pol II from promoter-proximal regions into gene bodies (*1*, *32*). We therefore evaluated the efficacy of candidate PAF1C inhibitors by performing RNA Pol II chromatin immunoprecipitation and sequencing (ChIP-seq) in HCT116 cells following 20 μM candidate inhibitor treatment. RNA Pol II release was assessed by calculating the pause-release ratio (PRR), which is the ratio of RNA Pol II occupancy level over the gene body to that of the promoter region (fig. S1A). As a positive control, *PAF1* expression was silenced in HCT116 cells using short hairpin RNA (shRNA) that we have used in our prior studies (*32*). The empirical cumulative distribution function (ECDF) of the PRR revealed several compounds that induced global release of paused RNA Pol II from promoter-proximal sites (fig. S2A). Of these, NUiPAF#22R-26 or *N*-(4-bromo-3-methylphenyl)-1-{1-[(3-fluorophenyl)methyl]-1*H*-1,3-benzodiazol-2-yl} piperidine-4-carboxamide (from this point forward named iPAF1C) was the best in class, closely mimicking the effect of *PAF1* shRNA transduction both globally (Fig. 1B and fig. S2A) and at individual gene bodies (Fig. 1C and fig. S2B).

To confirm that iPAF1C binds specifically to CTR9, we performed a cellular thermal shift assay (CETSA) in mock or iPAF1C-treated HCT116 cells (*53*). Immunoblot analysis demonstrated that iPAF1C enhanced CTR9 thermostability relative to dimethyl sulfoxide (DMSO) treatment (Fig. 1D). Notably, iPAF1C treatment had a limited thermostabilizing effect on the other PAF1C subunits, suggesting that iPAF1C specifically binds CTR9 (fig. S1, B and C). To confirm the inhibitory effect of iPAF1C on the interaction between PAF1 and CTR9, we performed PAF1 immunoprecipitation in DMSO or iPAF1C-treated DLD1 cells, engineered to express an auxin-inducible degron (AID) tag at the C terminus of the endogenous *PAF1* locus (*1*). Immunoblot analysis demonstrated that iPAF1C treatment disrupted the otherwise strong interaction between CTR9 and PAF1 seen in control-treated cells (fig. S1D).

Given that iPAF1C disrupts PAF1C nucleation and induces RNA Pol II release into gene bodies, we next examined the consequences of PAF1C disruption on global PAF1 chromatin occupancy by performing PAF1 ChIP-seq following treatment with either iPAF1C or the DMSO control. PAF1 chromatin occupancy was assessed over Pol II–transcribed genes covering a region spanning from 2 kb upstream to 3 kb downstream of the TSS. Metagene plot analysis demonstrated a marked reduction of PAF1 occupancy over 6938 RNA Pol II–transcribed genes following iPAF1C treatment (Fig. 1E). Moreover, a structurally homologous compound (NUiPAF#22R-26; an inactive version) was found to affect neither PAF1 chromatin levels nor global RNA Pol II pause-release, further confirming the specificity of iPAF1C (figs. S1E and S2A). As illustrated by a representative track following PAF1 ChIP-seq, iPAF1C markedly reduced PAF1 levels compared to DMSO- or NUiPAF#22R-26–treated cells (Fig. 1F). Together, these data suggest that iPAF1C is a specific small-molecule inhibitor that disrupts PAF1 complex formation by targeting the PAF1 binding pocket of CTR9, leading to reduced PAF1 chromatin occupancy

and release of paused RNA Pol II from promoter-proximal regions into gene bodies.

### PAF1C disruption via iPAF1C treatment impairs HS-induced RNA Pol II pausing

The cellular HS response involves genome-wide transcriptional changes, with rapid down-regulation of most genes but marked up-regulation of only a limited set of HS-responsive genes (*54*). Transcriptional repression of the HS–down-regulated genes was previously demonstrated to be a consequence of increased promoter-proximal pausing with PAF1C involvement in the process (*1*, *54*, *55*). Therefore, to further validate the functionality of iPAF1C in regulating RNA Pol II pause-release, we examined its effect on RNA Pol II pausing following HS. To this end, we exposed iPAF1C-treated DLD1 cells to HS stress for 1.5 hours and analyzed the resultant transcriptional effects by Precision Run-On sequencing (PRO-seq) (Fig. 2A). In these cells, we identified 652 genes that were down-regulated under the HS conditions, as indicated by decreased PRO-seq signal over gene bodies (Fig. 2B). ECDF plot of PRO-seq signals over down-regulated genes revealed increased RNA Pol II pausing upon HS (Fig. 2C), as further illustrated by track examples (Fig. 2D). As expected, iPAF1C treatment resulted

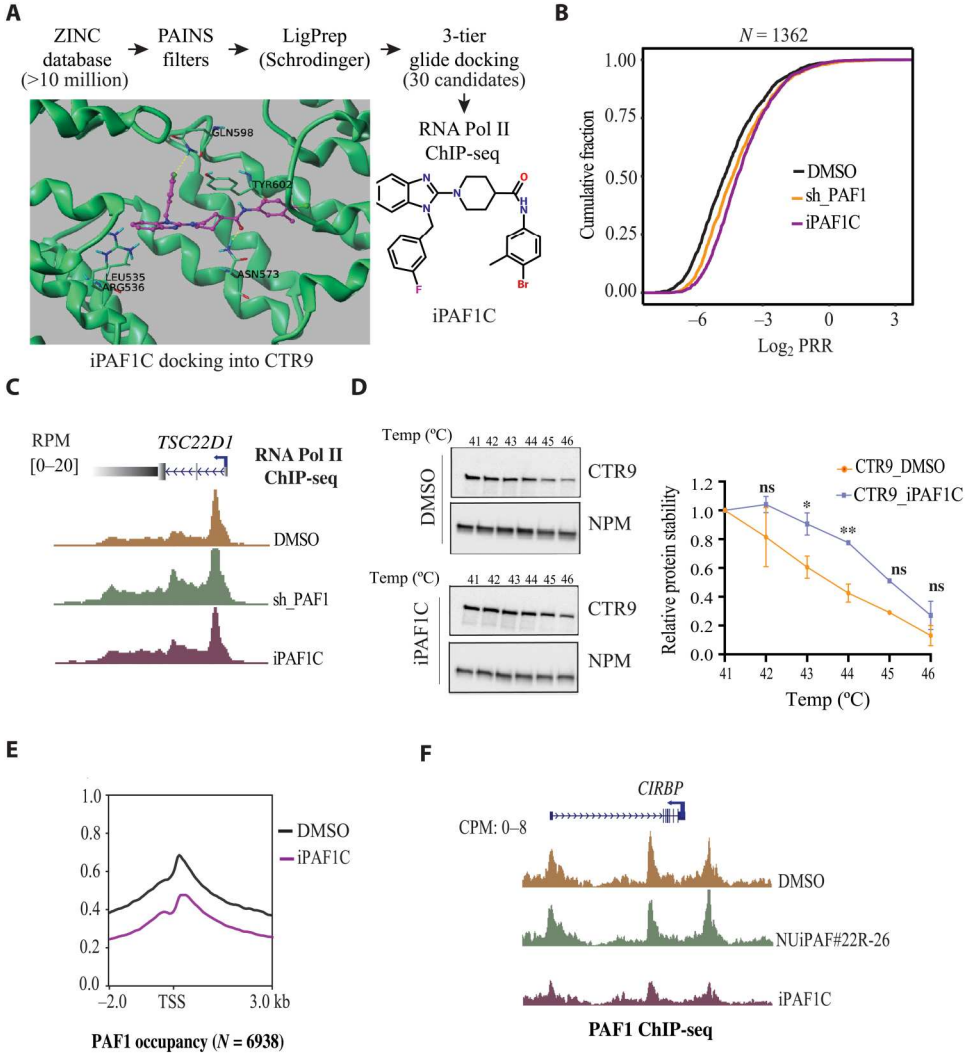


**Fig. 1. Structure-based identification of a small-molecule PAF1 complex (PAF1C) inhibitor that impairs PAF1 chromatin localization and releases RNA Pol II.** (**A**) Schematic representation of the structure-based identification of small-molecule disruptors of PAF1 and CTR9 interactions using in silico screen followed by RNA Pol II ChIP-seq screening. iPAF1C binding residues of CTR9 are shown. (**B**) Empirical cumulative distribution function (ECDF) plot illustrating $\log_2$ of RNA Pol II pause-release ratio (PRR) in HCT116 cells treated with either DMSO or 20 μM iPAF1C for 16 hours. $N = 1362$ genes. (**C**) Representative track demonstrating the ChIP-seq signal of RNA Pol II at *TSC22D1* in HCT116 cells treated with either DMSO or 20 μM iPAF1C for 16 hours. Cells transduced with shRNA targeting *PAF1* were used as a positive control. (**D**) Cellular thermal shift assay (CETSA) in HCT116 cells treated with either DMSO or 20 μM iPAF1C for 3 hours. Relative quantification of CTR9 protein is shown (average ± SD, $N = 2$ replicates). Analysis of statistical significance was performed by Student's *t* test: not significant (ns), $P > 0.06$; *$P < 0.06$; **$P < 0.01$. (**E**) Meta plot demonstrating genome-wide PAF1 occupancy levels over Pol II–transcribed genes in DLD1 cells treated with either DMSO or 20 μM iPAF1C. PAF1 levels are shown around 2 kb upstream of the TSS and up to 3 kb downstream TSS. $N = 6938$ genes. $N = 3$ replicates. (**F**) Track examples of UCSC genome browser demonstrating PAF1 occupancy as ChIP-seq signal at the promoter (indicated by blue arrow) and gene body of *CIRBP* gene following treatment with DMSO, iPAF1C, or its structural homolog NUiPAF#22R-26. Reads per million (RPM) is indicated on the *y* axis. CPM, counts per million.

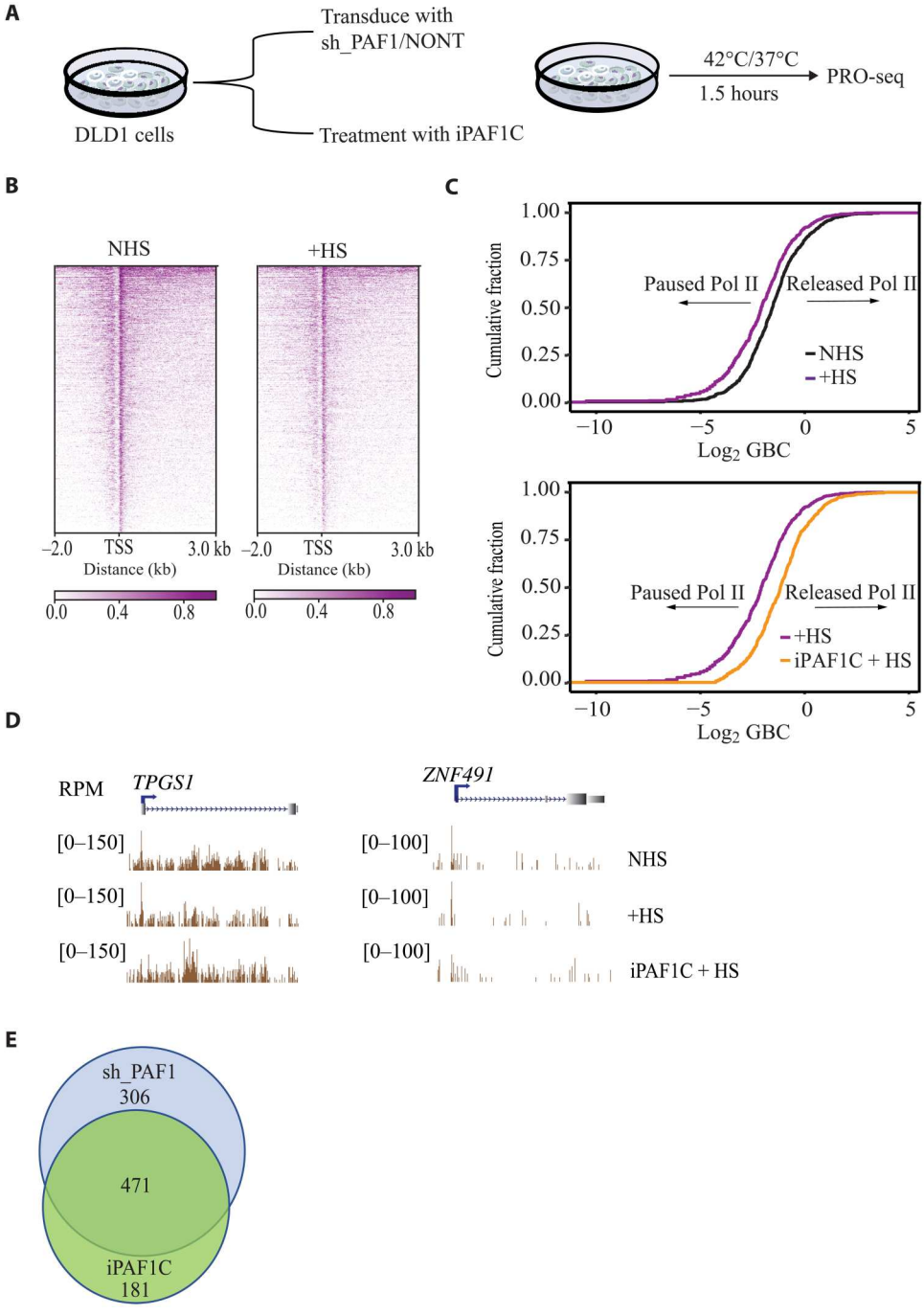


**Fig. 2. iPAF1C reduces RNA Pol II pausing at HS–down-regulated genes.** (**A**) Workflow of DLD1 cells infected with a lentiviral vector expressing shRNA against *PAF1* (sh_PAF1) or NONT control for 72 hours. The cells were treated with either DMSO or 20 μM iPAF1C for 16 hours before HS at 42°C for 1.5 hours and then collected for analysis via PRO-seq. (**B**) Heatmap demonstrating PRO-seq signal at 2 kb upstream of the TSS and in gene bodies of HS–down-regulated genes (up to 3 kb downstream of the TSS) in DLD1 cells treated with DMSO. NHS, non-HS. *N* = 652 genes. (**C**) ECDF plots demonstrating gene body coverage (GBC) of PRO-seq signal at 652 HS–down-regulated genes in DMSO-treated DLD1 cells (top) or iPAF1C (bottom) in HS and NHS conditions. (**D**) Representative track examples of PRO-seq signal at HS–down-regulated genes in DMSO-treated DLD1 cells (NHS versus +HS) or cells treated with 20 μM iPAF1C followed by HS (iPAF1C + HS). Normalized RPMs are shown. (**E**) Venn diagram demonstrating the overlap between genes displaying impaired RNA Pol II pausing upon *PAF1* knockdown (sh_PAF1) or iPAF1C treatment followed by HS.

in impaired RNA Pol II pausing in response to HS (Fig. 2, C and D). As a positive control, we generated DLD1 cell lines stably expressing a *PAF1*-targeting shRNA (shPAF1) or nontargeting shRNA (NONT). Using PRO-seq, we identified 777 genes down-regulated in the HS condition in NONT cells, a response severely dampened in shPAF1-expressing cells (fig. S3, A to C). Comparing these analyses, we saw a broad overlap between the effects of the iPAF1C-treated and *PAF1*-knockdown conditions (Fig. 2E). Together, these data establish that iPAF1C impairs RNA Pol II pausing in response to HS.

## iPAF1C-driven transcriptional changes resemble acute depletion of PAF1

To test whether iPAF1C-mediated disruption of PAF1C chromatin occupancy phenocopies PAF1 depletion, we used RNA Pol II ChIP-seq and RNA sequencing (RNA-seq) to compare the effects of iPAF1C and PAF1 degradation–inducing auxin treatment in DLD1_PAF1-AID cells (*1*). As seen in HCT116 cells, iPAF1C treatment resulted in the release of RNA Pol II into gene bodies, impaired PAF1 chromatin occupancy, and increased mRNA transcript abundance (Fig. 3A and fig. S4A). We observed both up-regulated and down-regulated genes upon acute depletion of PAF1, consistent with the previously established role of PAF1 as both a positive and negative regulator of transcription elongation (Fig. 3B). However, most of the differential expression observed in response to PAF1 depletion or iPAF1C treatment was up-regulation, indicating greater prevalence of PAF1's role as a negative regulator of RNA Pol II pause-release, as previously reported (*1*, *34*). Treatment with iPAF1C largely phenocopied the transcript abundance changes observed upon auxin-induced PAF1 depletion (Fig. 3B). Moreover, global analysis of RNA Pol II chromatin occupancy levels at these loci revealed increased RNA Pol II occupancy over gene bodies of most genes, further validating the association between impaired PAF1 chromatin recruitment and iPAF1C-induced release of RNA Pol II in the function of iPAF1C (Fig. 3C). Last, relative log expression (RLE) analysis suggested that the magnitude of the change among up-regulated genes was similar between the auxin- and iPAF1C-treated cells (Fig. 3D). In summary, these data suggest that iPAF1C treatment closely phenocopies the transcriptional impacts of acute PAF1 depletion.

## iPAF1C enhances HIV-1 latency reactivation upon LRA treatment

PAF1C was previously implicated to play a role both in the negative regulation of HIV-1 transcription during active replication and in transcriptional silencing of integrated proviruses during the

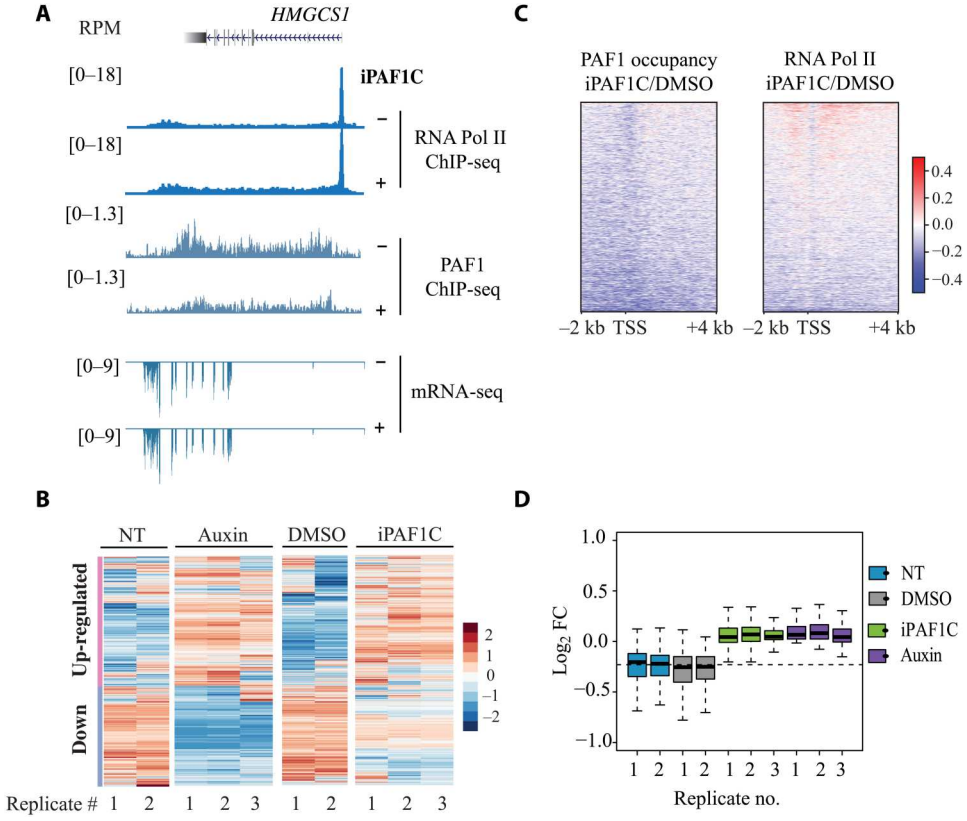


**Fig. 3. iPAF1C-driven transcriptional changes resemble acute depletion of PAF1.** (**A**) Representative tracks of RNA Pol II ChIP-seq (top), PAF1 ChIP-seq (middle), and poly(A)-enriched mRNA-seq signals (bottom) of *HMGCS1* gene in DLD1-PAF1_AID cells. Cells were treated with either 20 μM iPAF1C compared to DMSO or 500 μM auxin versus nontreated (NT). $N = 3$ replicates. (**B**) Heatmap demonstrating $\log_2$ fold change (FC) for gene expression in DLD1-PAF1_AID cells treated as in (A). $N = 4621$ genes. The number of independent replicates is indicated. (**C**) Heatmap of $\log_2$ FC for PAF1 and RNA Pol II occupancy levels in iPAF1C- versus DMSO-treated cells over Pol II– and PAF1-transcribed genes. $N = 4342$ genes. (**D**) Relative log expression (RLE) plot for up-regulated differentially expressed genes in DLD1-PAF1_AID cells. Cells were treated with DMSO versus 20 μM iPAF1C or nontreated (NT) versus 500 μM auxin [that result in the loss of PAF1(PAF1AID)].

establishment and maintenance of latency (*39*). To test the impact of iPAF1C on HIV-1 replication, we isolated $CD4^+$ T cells from the blood of three healthy human donors. Cells were activated for 72 hours with anti-CD3/anti-CD28 antibodies and pretreated with iPAF1C over a range of concentrations before challenge with HIV-1 NL4.3 Nef–internal ribosomal entry site (IRES)–green fluorescent protein (GFP). Increasing concentrations of iPAF1C increased the infected cell populations in a dose-dependent manner, although at high concentrations decreased infection was observed, concomitant to decreased cell viability (Fig. 4A and fig. S5A).

Given the role of PAF1C in the maintenance of transcriptional latency, we next sought to determine the potential use of iPAF1C as a latency reversal agent (LRA) using the J-Lat 5A8 cell line latency

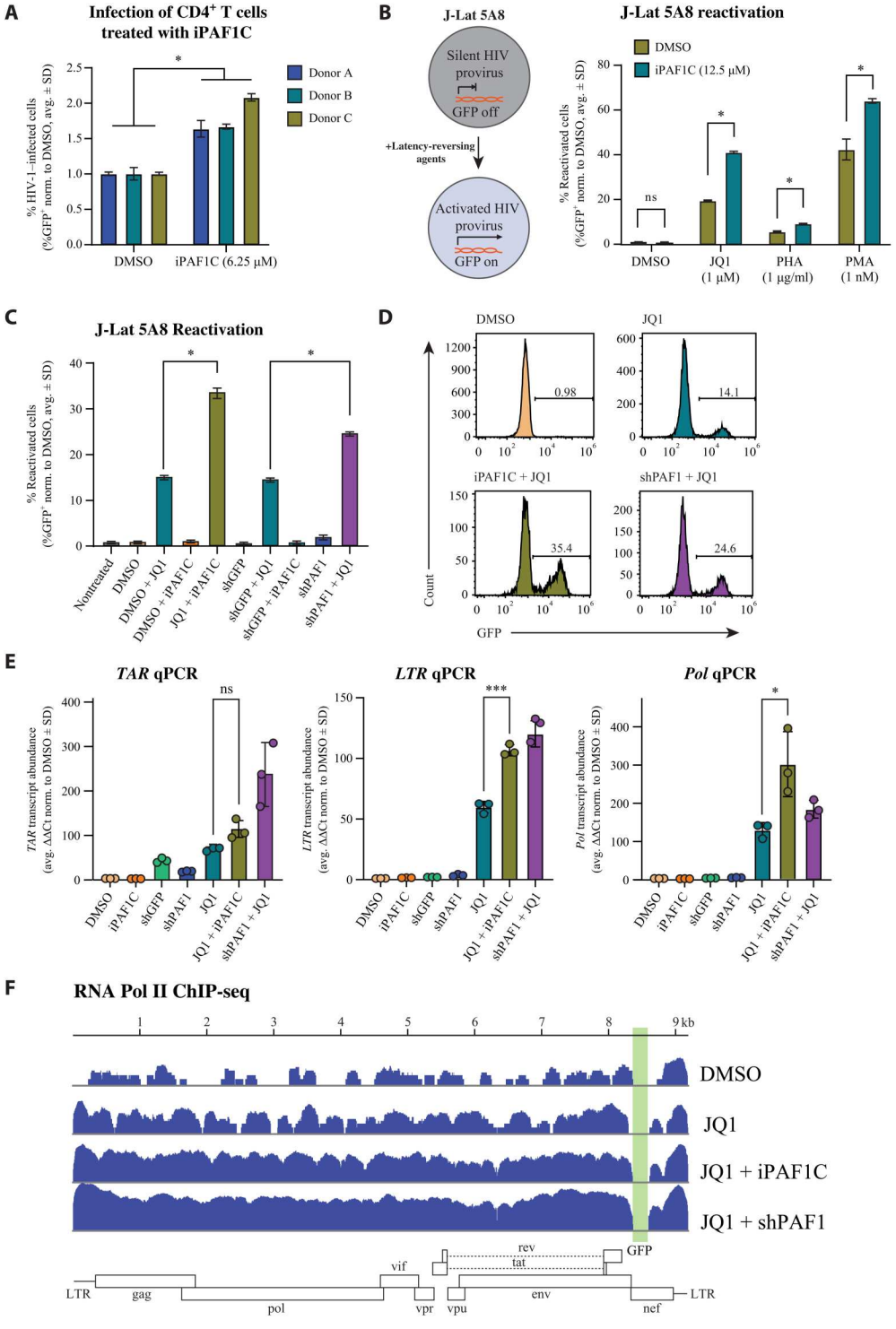


**Fig. 4. iPAF1C enhances the activity of LRAs by enhancing transcriptional elongation of integrated HIV-1 proviruses.** (**A**) Percent of infected ($GFP^+$) primary human $CD4^+$ T cells pretreated with either iPAF1C (6.25 μM) or DMSO 48 hours after challenge with HIV-1 NL4.3 Nef-IRES-GFP. Data represent the average ± SD of technical triplicates normalized to the DMSO, $n = 3$ donors; $^*P < 0.05$ (Welch's *t* test). (**B**) Schematic of the J-Lat latency reversal assay (left) and percent reactivated ($GFP^+$) J-Lat 5A8 cells 48 hours after treatment with each compound (right). Data represent the average ± SD of technical triplicates normalized to the DMSO; $^*P < 0.05$; ns, $P > 0.05$ (Welch's *t* test). (**C**) Percent reactivated ($GFP^+$) J-Lat 5A8 cells 48 hours after treatment with the indicated compounds. Stable knockdown J-Lat 5A8 cells were generated by lentiviral transduction with shRNA targeting *PAF1* or *GFP* (control). Data represent the average ± SD of technical triplicates normalized to the DMSO; $^*P < 0.05$; ns, $P > 0.05$ (Welch's *t* test). (**D**) Representative flow cytometry histograms depicting GFP fluorescence in J-Lat 5A8 cells 48 hours after each treatment. (**E**) *TAR* (left), *LTR* (middle), or *Pol* (right) transcript abundance in J-Lat 5A8 cells 48 hours after treatment with each compound as measured by qRT-PCR. Data represent the average $\Delta\Delta Ct\ [(Ct_{target} - Ct_{\beta\text{-actin}})_{EXPT} - (Ct_{target} - Ct_{\beta\text{-actin}})_{DMSO}] \pm SD$ of technical triplicates; $^*P < 0.05$; $^{***}P < 0.005$; ns, $P > 0.05$ (Welch's *t* test). (**F**) RNA Pol II ChIP-seq tracks over the integrated HIV-1 viral gene body in J-LAT 5A8. Viral open reading frames are indicated below, and the location of the integrated GFP reporter is indicated in green.

model; these cells are a subclone of Jurkat T cells that harbor a transcriptionally silent, integrated provirus with a GFP reporter (Fig. 4B). Increasing concentrations of iPAF1C resulted in minimal reactivation up to 12.5 μM, at which point the cells exhibited viability defects (fig. S5B). It is known that blocks at multiple different steps of transcription can maintain and influence HIV-1 latency (*56*), so we next tested whether iPAF1C could enhance the activity of well-characterized LRAs including the bromodomain inhibitor JQ1 (*57*), the T cell stimulatory lectin phytohemagglutinin (PHA), and the protein kinase C (PKC) agonist phorbol 12-myristate 13-acetate (PMA). Notably, iPAF1C significantly enhanced the activity of each of these three LRAs not only in J-Lat 5A8 cells (Fig. 4B) but also in J-Lat clones 11.1 and 6.3 (fig. S5C). This enhanced latency reversal was not due to a negative effect on cell viability (fig. S5D). Knockdown of *PAF1* in J-Lat 5A8 cells by shRNA had no impact on its own, but the knockdown condition enhanced JQ1-induced reactivation, similar to iPAF1C treatment (Fig. 4, C and D).

It has been hypothesized that PAF1C inhibits HIV transcription by enforcing promoter-proximal pausing and by disrupting transcriptional elongation. To test the impact of iPAF1C on stages of proviral transcription, we used quantitative reverse transcription polymerase chain reaction (qRT-PCR) to quantify viral RNA using probes for the *Trans-Activation Response* (*TAR*) stem loop, which is synthesized upon transcription initiation, and for the *LTR* and Pol transcripts, which are synthesized during transcriptional elongation (*58*). Although JQ1 treatment increased *TAR*, *LTR*, and *Pol* transcript abundance, neither iPAF1C treatment nor shRNA knockdown of *PAF1* was alone sufficient to affect a similar increase (Fig. 4E). However, combined treatment with JQ1 + iPAF1C significantly increased levels of *LTR* and *Pol* transcription beyond that seen after JQ1 treatment alone; however, this boosting effect was not seen for *TAR* transcripts, indicating that iPAF1C acts to boost the activity of the LRA JQ1 specifically by lifting a block on transcriptional elongation (Fig. 4E). That being said, the combination of iPAF1C and several LRAs did result in significant increases in both *TAR* and *LTR* transcripts, suggesting that iPAF1C may also affect transcriptional initiation in some contexts (fig. S5E).

To further characterize the impact of iPAF1C on proviral expression in J-Lat 5A8 cells, we performed RNA Pol II ChIP-seq following treatment with DMSO, JQ1, or JQ1 + iPAF1C (Fig. 4F). In the DMSO-treated cells, decreased RNA Pol II signal was observed in the proviral gene body. However, treatment with JQ1 increased RNA Pol II both at the *LTR* and throughout the provirus, and the combination of JQ1 and iPAF1C treatment resulted in a further increase in RNA Pol II occupancy throughout the proviral genome. This same boosting effect was observed in PAF1 knockdown cells treated with JQ1 (Fig. 4F). Together, these data suggest that iPAF1C enhances the activity of HIV LRAs through the release of promoter-proximally paused RNA Pol II and enhancement of transcriptional elongation.

### Ex vivo iPAF1C treatment of PBMCs from persons living with HIV-1 results in latency reversal

Following the observation that iPAF1C works synergistically with LRAs across multiple cell line models of HIV-1 latency, we next tested whether this compound could reverse latency, either alone or in combination with LRAs, in cells from persons living with HIV-1 (PLWH) (Fig. 5A). Human peripheral blood mononuclear cells (PBMCs) were obtained from the whole blood of four PLWH enrolled in the Northwestern University Clinical Research Site for the MACS/WIHS Combined Cohort Study (MWCCS). The selected PLWH had been virally suppressed for more than 5 years, with undetectable HIV-1 plasma levels at the time of blood draw (<50 copies/ml) (Fig. 5B). Cells from these samples were then treated for 48 hours with DMSO, JQ1, PHA, or PMA, alone or in combination with iPAF1C. RNA from the treated cells was isolated, and the reactivation of viral gene expression was quantified by HIV-1 *gag* levels through qRT-PCR (Fig. 5C). In contrast to the cell line models, we observed that treatment of these cells with iPAF1C alone resulted in a significant increase of HIV-1 *gag* transcript levels. Consistent with our results in cell line models, we observed that while JQ1 alone induced latency reactivation, JQ1 + iPAF1C resulted in significantly increased activity. Together, these data suggest a model whereby iPAF1C disrupts PAF1C nucleation on chromatin, resulting in the release of proximally paused RNA Pol II at the HIV-1 proviral promoter to enhance LRA activity (Fig. 5D).

## DISCUSSION

In this study, we report the identification of a first-in-class small molecular disruptor of the PAF1 complex (iPAF1C), which targets the highly conserved interaction interface between PAF1 and CTR9 to disrupt complex assembly. Inhibition of the PAF1-CTR9 interaction by iPAF1C impairs the genome-wide chromatin occupancy of PAF1 and induces global release of RNA Pol II from the promoter-proximal region into gene bodies. These effects of iPAF1C closely mimic the effects of either *PAF1* knockdown by shRNA or acute PAF1 depletion in a PAF1-AID degron system, demonstrating specificity of the compound for PAF1C. Likewise, iPAF1C treatment causes changes in global gene expression similar to those seen upon acute depletion of PAF1. Mapping nascent RNA transcripts at single-nucleotide resolution by PRO-seq revealed that, analogous to the acute depletion of PAF1, iPAF1C impairs the cellular response to stimuli, exemplified by HS, by attenuating RNA Pol II pausing at HS–down-regulated genes. Last, iPAF1C increases the efficiency of a broad array of HIV LRAs both in cell line models and in patient cells by enhancing transcriptional elongation. This first-in-class molecular disruptor of PAF1C provides previously unexplored molecular tool for altering the chromatin-dependent functions of PAF1, enabling us to better understand the functions both of this complex and of RNA Pol II proximal promoter pausing in diverse disease states.

One major obstacle in targeting PAF1C was the lack of either trackable enzymatic activity or a conserved active site. We overcame this limitation by taking an alternative approach of disrupting PAF1 complex formation by targeting the conserved interaction between the subunits PAF1 and CTR9, which is essential for the complex integrity. Prior structural studies of the highly conserved Ctr9, Paf1, and Cdc73 ternary complex using full-length proteins from the thermophilic fungi *Myceliophthora thermophila* (PDB: 6AF0) suggested a spirally wrapped interface with Paf1 binding to a Ctr9 groove (*26*). The primary sequence and cryo-EM structure of human CTR9 (PDB: 6GMH; PDB: 5ZYQ) suggested conservation of this binding pocket and amenability to small-molecule disruption (*29*). In agreement with these findings, our visual analysis of the human CTR9-PAF1 crystal structure (PDB: 5ZYQ) (*27*) revealed the presence of a highly conserved groove of the CTR9

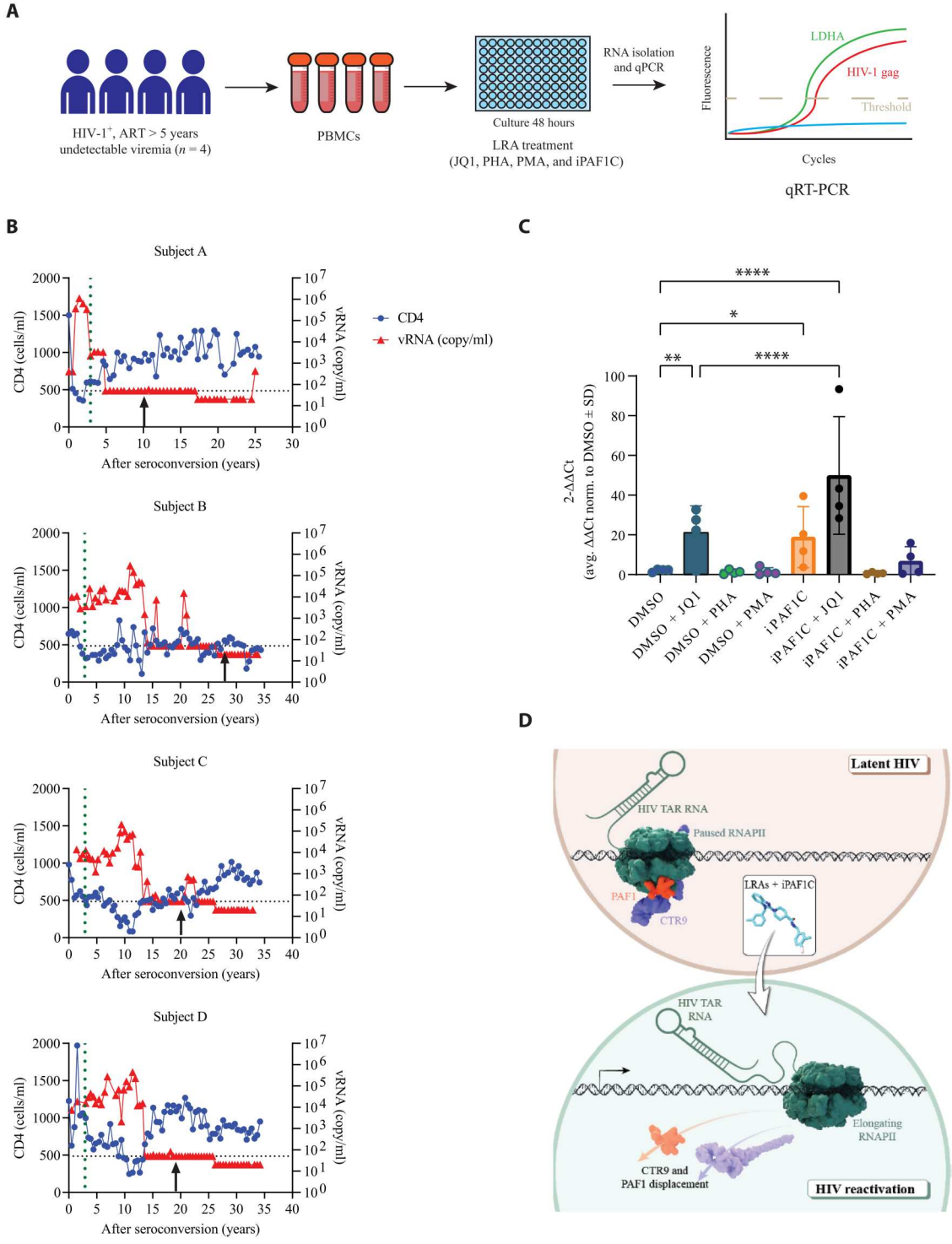


**Fig. 5. iPAF1C reverses latency in PBMCs from PLWH.** (**A**) Graphical illustration of experimental design. PBMCs were isolated from patients with undetectable levels of HIV-1 and treated with iPAF1C, PMA, PHA, and JQ1. HIV-1 transcriptional reactivation was measured by qRT-PCR. (**B**) Graphs depicting CD4 count (blue) and levels of detectable viral RNA (red) over time. The time of Antiretroviral Therapy (ART) initiation is depicted by a green dotted line, and the time of blood draw used for the latency reversal treatments is depicted in the figure by an arrow. (**C**) HIV-1 *gag* mRNA transcripts by qRT-PCR in PBMCs isolated from four patients of HIV and treated with DMSO, JQ1, PHA, or PMA in the presence or absence of iPAF1C. Data represent the average $\Delta\Delta$Ct $[(Ct_{target} - Ct_{LDHA})_{EXPT} - (Ct_{target} - Ct_{LDHA})_{DMSO}] \pm$ SD of the four patients; $^{*}P < 0.05$; $^{**}P < 0.01$; $^{****}P < 0.0001$ [analysis of variance (ANOVA) with Tukey multiple comparisons test]. (**D**) Putative model for HIV-1 latency reversal by iPAF1C. Treatment with iPAF1C results in disruption of PAF1C complex integrity and delocalization of PAF1 from the chromatin, resulting in release of RNA Pol II (RNAPII) into the proviral gene body and increased transcription.

subunit interacting with PAF1 (Fig. 1A). A virtual screen using simulated molecular docking of potential inhibitors into the PAF1 binding groove of CTR9 identified 30 candidates for synthesis and functional testing by in vivo chromatin occupancy studies (Fig. 1, D and E, and fig. S1D). The cellular effects of iPAF1C on RNA Pol II chromatin occupancy and transcript abundance were largely mimicked by PAF1 depletion using two orthogonal approaches (Fig. 3B).

Previously, we and others have systematically examined the role of PAF1C in orchestrating several stages of transcription. These studies demonstrated the essential role of PAF1C in maintaining RNA Pol II pausing, a role that PAF1C appears to play specifically at the second pause site (*1*, *32*, *59*). Here, our results show that iPAF1C induces global RNA Pol II pause-release similar to that seen upon PAF1 knockdown (Fig. 1B). It was recently reported that while PAF1 depletion leads to RNA Pol II release and up-regulation of short genes, transcripts from longer gene bodies are mostly down-regulated, due to decreased RNA Pol II processivity and premature termination (*15*, *34*). Our global transcriptomic studies following iPAF1C treatment found that, while a majority of differentially expressed genes were up-regulated, a substantial proportion were also down-regulated, consistent with a dual role for PAF1C in regulating both pause-release and processivity (Fig. 3B). Molecular studies from yeast to human have also shown that PAF1C affects histone posttranslational modifications (PTMs) by recruiting additional histone-modifying factors such as RAD6/BRE1, DOT1L, and SETD2 (*20*, *22*, *60*–*63*). Disruption of these modifications could also result in transcriptional down-regulation despite decreased RNA Pol II pausing, but more studies are needed to establish the effect of iPAF1C on histone PTMs.

Genome-wide transcriptional repression in response to HS occurs at over ~8000 genes, while specific response genes, which are up-regulated, number only in the few hundreds (*54*). The transcriptional repression of a large subset of the genes down-regulated in response to HS can be attributed to an increase in promoter-proximal pausing (*1*, *54*). On the other hand, repression of another subset of HS–down-regulated genes is reportedly attributable to the combination of an increase in RNA Pol II elongation rate and decreased processivity, leading to premature transcript termination (*64*). Our PRO-seq data show the HS-induced accumulation of RNA Pol II at TSS of a subset of HS–down-regulated genes with an accompanying decrease in signal at their gene bodies (Fig. 2D and fig. S3C). These data indicate the increase of RNA Pol II pausing at these specific genes, consistent with the previously reported role of RNA Pol II pause-release regulation in the HS response. The iPAF1C treatment resembled PAF1 knockdown in its effects, impairing RNA Pol II accumulation at TSS and increasing elongating Pol II in the vicinity of these genes (Fig. 2D and fig. S3C). These data confirm the specific effect of iPAF1C on PAF1C function in response to cellular stimuli. The compound can also be used in future studies to determine how PAF1C affects RNA Pol II processivity and how this impact may differ by gene body.

The PAF1 complex has previously been implicated in negatively regulating HIV transcription during both active replication and latency (*39*). While iPAF1C alone did not reactivate viral transcription in cell line models of latency, it was sufficient to increase the levels of cell-associated viral RNA in PBMCs isolated from virally suppressed PLWH. These data are consistent with the model that blocks to transcriptional elongation are one of several potentially concurrent modes of latency regulation (*13*). While PAF1C may be the major hurdle in some cells, for example, patient cells with a diverse population of latent proviruses, it represents only one of many blocks that may be present in more homogeneous cell line models. That PAF1C negatively regulates HIV transcription is further supported by the ability of iPAF1C to enhance the reactivation potential of diverse LRAs including PHA, PMA, and JQ1 across different latency models. JQ1 is a BET inhibitor hypothesized to promote latency reversal by increasing the level of active P-TEFb and by depleting BRD2, which halts Pol II at the viral promoter (*57*, *65*). We speculate that the enhanced availability of P-TEFb due to JQ1 treatment increases transcriptional initiation, while iPAF1C removes blocks to transcriptional elongation, enabling synergistic reactivation of latent proviruses (*1*). More mechanistic study of PAF1C's role in regulating HIV latency maintenance and establishment will better inform our understanding of the latent state and future formulations of latency-targeting therapeutics.

In sum, this study identifies iPAF1C as a first-in-class iPAF1C formation. This inhibitor is a valuable tool that will facilitate the study of both PAF1C and transcriptional elongation control under diverse physiological conditions and disease states. The therapeutic potential of iPAF1C to regulate the transcriptional machinery is illustrated by its facilitation of HIV latency reversal. PAF1C has also been implicated as an oncogenic factor in several cancers (*66*–*70*); the therapeutic potential of iPAF1C to control tumor cell proliferation and oncogenic transcriptional programs will be an important area of future investigation.

## MATERIALS AND METHODS

### Cell lines and cell culture

DLD1 [American Type Culture Collection (ATCC), CCL-221] and HCT116 cells (ATCC, CCL-247) were maintained in Dulbecco's modified Eagle's medium (Sigma-Aldrich, catalog no. D6429) supplemented with 10% fetal bovine serum (FBS) (Sigma-Aldrich, catalog no. F2442). J-Lat 5A8 [National Institutes of Health (NIH) AIDS Reagent Program], J-Lat 11.1, and J-Lat 6.3 (gift from R. D'Aquila) were cultured in RPMI 1640 (Sigma-Aldrich, catalog no. R8758) supplemented with 5 mM Hepes (Corning, catalog no. 25-060-Cl), penicillin-streptomycin (50 μg/ml; Corning, catalog no. 30-002-Cl), 5 mM sodium pyruvate (Corning, catalog no. 25-000-Cl), and 10% FBS (Gibco, catalog no. 10082147). Cells were cultured at 37°C in a humidified incubator with 5% $CO_2$. For RNA interference, cells were infected with a lentivirus containing shRNA against PAF1 using polybrene (8 μg/ml) for 24 hours followed by puromycin (2 μg/ml) for 2 days. The shRNAs were purchased from Open Biosystems. The clone ID for shPAF1 is TRCN0000005454.

### In silico high-throughput screening

The ZINC database containing about 40 million commercially available small molecular inhibitors (*52*) were used for performing virtual high-throughput screening. The available molecules were filtered using PAINS substructures with Smiles ARbitrary Target Specifications strings (*71*). PAINS filtering generated 10 million available small molecules to be further screened. Those molecules were then subjected to the LigPrep module of Schrodinger (Small-Molecule Drug Discovery Suite 2017-2, Schrödinger LLC, New York) in OPLS2005 force field at pH 7.4 ± 1 (physiological

pH) retaining the specific chirality. This ligand preparation panel that generated a low energetic three-dimensional structure for each molecule was generated in this ligand preparation panel. Each potential molecule was validated by performing RNA Pol II ChIP-seq.

### Chromatin immunoprecipitation sequencing

ChIP-seq was performed according to a previously published protocol (*72*). Briefly, culture media were aspirated and about 20 million to 50 million of cells were washed twice with ice-cold 1× phosphate-buffered saline (PBS; Thermo Fisher Scientific, catalog no. 14190250) and then cross-linked with 1% paraformaldehyde (Thermo Fisher Scientific, catalog no. 28908) for 10 min while shaking at room temperature. The reaction was quenched using 0.2 M glycine (Fisher Scientific, catalog no. BP381-5) for 5 min at room temperature followed by centrifugation at 1350 rpm for 5 min. Successively, cells were gently washed with ice-cold PBS and centrifuged at 1350 rpm for 5 min. For RNA Pol II and PAF1 ChIP-seq, the chromatin was sonicated using Covaris E220 for 4 min using the following sonication conditions: 10% duty cycle, 140 peak intensity power, and 200 cycles per burst. Successively, pulldown of chromatin was carried out overnight at 4°C using the specific antibodies [Rpb1 NTD (D8L4Y) rabbit monoclonal antibody for RNA Pol II and PAF1 (D9G9X) rabbit monoclonal antibody]. Next day, Dynabeads protein G (Invitrogen, catalog no. 10004D) were added to the immunoprecipitation mix and incubated at 4°C for 4 hours. Nonspecific proteins were washed away, and bead-bound proteins were digested using proteinase K (400 mg/ml; Roche, catalog no. 3115828001). Reverse cross-linking was performed at 65°C overnight while shaking at 1200 rpm. Immunoprecipitated DNA was extracted using phenol-chloroform (Thermo Fisher Scientific, catalog no. 17909) followed by ethanol precipitation and washing. DNA was dissolved in 10 mM tris-HCl (pH 8) and quantified using Qubit. DNA libraries were prepared by the HTP Library Preparation Kit for Illumina (KAPA) and sequenced on NextSeq 500 or NovaSeq 6000 (Illumina) in the single-end (SE) mode. Preprocessing was performed using CETO Toolbox (*73*); low-quality bases were removed using Trimmomatic v0.33 (*74*), with parameters TRAILING:30 MINLEN:20. Reads were aligned with Bowtie v1.1.2 (*75*, *76*), with parameters -m 1 -v 2, to human GRCh38 genome assembly with Ensembl gene annotation GRCh38 release 78. Bigwig files were generated using an in-house R script using bam2bw function, with a parameter to extend reads length -extLen = 150 and scaled to reads per million (RPM).

### RNA extraction, cDNA, and RNA-seq

Total RNA was extracted using an RNeasy Mini kit (Qiagen, catalog no. 74106). Briefly, 1 million of DLD1_PAF1_AID cells were plated in a six-well plate 24 hours before treatment with 20 μM iPAF1C versus DMSO or 500 μM auxin versus nontreated cells. We prepared cDNA from extracted RNA using a common RT reaction. SuperScript IV buffer (Invitrogen, catalog no. 18090050B) was used with random hexamers (50 μM). cDNA was synthesized following the manufacturer's protocol. For performing RNA-seq, polyadenylated [poly(A)$^+$] RNA was isolated using the NEBNext Poly(A) mRNA Magnetic Isolation Module [New England Biolabs (NEB), catalog no. E7490L]. This isolated poly(A)$^+$ RNA was used to prepare libraries using the NEBNext Ultra II Directional RNA Library Prep Kit (NEB, catalog no. E7760L). Libraries were sequenced on NovaSeq 6000 (Illumina) in the SE mode. Preprocessing was performed using CETO Toolbox (*73*); low-quality bases were removed using Trimmomatic v0.33 (*74*), with parameters TRAILING:30 MINLEN:20. Reads were aligned to human GRCh38 genome assembly with Ensembl gene annotation GRCh38 release 78 using TopHat2 v2.1.0 (*77*). Reads with nonprimary alignment and low mapping quality were discarded. Reads were quantified using HTSeq v0.6.1 (*78*). Raw read counts were normalized to remove technical differences and batch effects using RUVs 1.26.0 (*79*), which estimates unwanted variation using replicate samples. Differential expression analysis was performed using DESeq2 1.32.0; the model included normalization terms obtained from RUV analysis. Genes with adjusted $P$ values < 0.05 (the Benjamini and Hochberg method) and an absolute fold change > 25% were considered differentially expressed.

### Immunoprecipitation

Total cell lysates were extracted from DLD1_PAF1-AID cells using Triton lysis buffer containing 50 mM tris-HCl (pH 7.4), 150 mM NaCl, 1 mM EDTA, and 1% Triton X-100. Cell lysates were extracted in the presence of protease and phosphatase inhibitors (Thermo Fisher Scientific, catalog no. 78442). Briefly, cells were treated with either DMSO or 20 μM iPAF1C for 16 hours. As a positive and negative control, cells were treated with water or 500 μM auxin for 2 hours. Cell lysates were incubated in ice for 30 min followed by centrifugation at 10,000*g* for 20 min at 4°C. The supernatant was collected and incubated overnight with our homemade AID antibody at 4°C. Antibody-bound proteins were captured using Protein A/G PLUS-Agarose (Santa Cruz Biotechnology, catalog no. sc-2003). Unbound proteins were washed away by washing the beads four times at 4°C using Triton lysis buffer. Last, protein complexes were eluted by boiling the beads in 1× Laemmli sample buffer (Bio-Rad, catalog no. 1610747) at 98°C for 10 min followed by immunoblot.

### qPCR measurement of HIV-1 transcripts

Following cDNA synthesis, viral transcripts were assessed by qRT-PCR. For viral *TAR*, the following primers were used: PF: 5′-GTCTCTCTGGTTAGACCAG-3′; PR: 5′-TGGGTTCCCTAGYTAGCC-3′; and prob: 5′-AGCCTGGGAGCTC-3′. Viral *LTR* levels were assessed using the following primers: PF: 5′-GCCTCAATAAAGCTTGCCTTGA-3′; PR: 5′-GGGCGCCACTGCTAGAGA-3′; and prob: 5′-CCAGAGTCACACAACAGACGGGCACA-3′. Viral *Pol* levels were tested using the following primers: PF: 5′-GCACTTTAAATTTTCCCATTAGTCCTA-3′; PR: 5′-CAAATTTCTACTAATGCTTTTATTTTTTC-3′; and prob: 5′-AAGCCAGGAATGGATGGCC-3′. For expression level normalization, *ACTB* was used (Thermo Fisher Scientific, catalog no. 4331182). The reaction was performed using TaqMan Fast Advanced Master Mix (Thermo Fisher Scientific, catalog no. 4444557). The PCR cycles were done as follows: 95°C for 5 min followed by 40 cycles of 95°C for 15 s and 60°C for 30 s. Reactions were performed in triplicate.

### HS induction

HS of mammalian cells was performed using ~70 to 80% confluent DLD1 cells by adding preheated (42°C) conditioned media collected from identically growing cells (*54*). The HS cells were incubated at

42°C for 1.5 hours. After washing with PBS, the HS and non-HS DLD1 cells were processed for PRO-seq as described below.

### PRO-seq library preparation and alignment

PRO-seq was performed according to the previously published protocol with minor modifications (*80*). Briefly, HCT116 cells were treated with 20 μM iPAF1C or DMSO as a control. Knocking down PAF1 was achieved by transducing cells with a lentiviral vector expressing shRNA against PAF1. Following cell permeabilization, about 10 million HCT116 nuclei were mixed with 0.5 million spike-in *Drosophila* S2 cell nuclei. Nuclear run-on assays were performed with 25 mM Biotin-11-ATP/UTP/CTP/GTP (PerkinElmer) for 3 min at 30°C. RNA fragmentation was performed with 0.2 M NaOH for 10 min on ice. Biotin-labeled RNA was purified by streptavidin beads M-280 (Thermo Fisher Scientific, catalog no. 11205D). The 5′ cap removal and triphosphate repair were performed with RppH (NEB, catalog no. M0356); 50 hydroxyl repair was then performed with PNK (NEB, catalog no. M0201). The 5′ and 3′ adaptor ligation was performed with T4 RNA ligase I (NEB, catalog no. M0204). RT was performed with SuperScript III (Thermo Fisher Scientific, catalog no. 18080044). cDNA was amplified using Phusion Hot Start II DNA polymerase (Thermo Fisher Scientific, catalog no. F549). DNA libraries were purified using Beckman Coulter AMpure XP (Fisher Scientific, catalog no. NC9959336) and sequenced on NextSeq 500 (Illumina) in the SE mode. Low-quality bases and adapters from 30 ends of reads were removed using cutadapt 1.14 requiring a read length of 16 to 36 base pairs. Reads derived from ribosomal RNA were filtered out by mapping reads on human and fly ribosomal DNA. The remaining reads were aligned using Bowtie 2.2.6 (*75*) with option --very-sensitive, to a concatenated genome composed of human hg38 (sample) and fly dm6 (spike-in) assemblies. The 5′ ends of aligned reads with MAPQ 30 were processed using bedtools genomecov v2.25.0 (*81*) with parameters -strand, -bg, and -5 to calculate coverage of 5′ ends. Read counts were normalized with total reads aligned to the spike-in genome (dm6), and final bigwig files were scaled to RPM. J-Lat 5A8 cells were aligned to the concatenated hg38/HIV-1 genome, using the same parameters as for the human samples. After alignment, HIV-1 reads were filtered out and normalized by the mapped read counts.

### $CD4^+$ T cell isolation

Primary human $CD4^+$ T cells from healthy donors were isolated from leukoreduction chambers after Trima apheresis (STEMCELL Technologies). PBMCs were isolated by Ficoll centrifugation. Bulk $CD4^+$ T cells were subsequently isolated from PBMCs by magnetic negative selection using an EasySep Human $CD4^+$ T cell isolation kit (STEMCELL Technologies; per the manufacturer′s instructions). Isolated $CD4^+$ T cells were suspended in RPMI 1640 (Sigma-Aldrich) supplemented with 5 mM Hepes (Corning), penicillin-streptomycin (50 mg/ml; Corning), 5 mM sodium pyruvate (Corning), and 10% FBS (Gibco). Media were supplemented with interleukin-2 (IL-2; 20 IU/ml; Miltenyi) immediately before use. For activation, bulk $CD4^+$ T cells were immediately plated on anti-CD3–coated plates [coated for 2 hours at 37°C with anti-CD3 (20 mg/ml) (UCHT1; Tonbo Biosciences)] in the presence of soluble anti-CD28 (5 mg/ml; CD28.2; Tonbo Biosciences). Cells were stimulated for 72 hours at 37°C and 5% $CO_2$ before treatment with iPAF1C.

### Preparation of virus stocks for infection of primary $CD4^+$ T cell cultures

Replication-competent reporter virus stocks were generated from an HIV-1 NL4-3 molecular clone in which GFP had been cloned behind an IRES cassette following the viral nef gene (NIH AIDS Reagent Program, catalog no. 11349). Briefly, 10 mg of the molecular clone was transfected (PolyJet; SignaGen) into $5 \times 10^6$ human embryonic kidney (HEK) 293T cells (ATCC, CRL-3216) according to the manufacturer′s protocol. Twenty-five milliliters of the supernatant was collected at 48 and 72 hours and then combined. The virus-containing supernatant was filtered through 0.45-mm polyvinylidene difluoride filters (Millipore) and precipitated in 8.5% polyethylene glycol [average molecular weight (Mn), 6000; Sigma-Aldrich] and 0.3 M NaCl for 4 hours at 4°C. Supernatants were centrifuged at 3500 rpm for 20 min, and the virus was resuspended in 0.5 ml of PBS for a 100× effective concentration. Aliquots were stored at −80°C until use.

### HIV-1 infection of primary $CD4^+$ T cell cultures treated with iPAF1C

Activated primary $CD4^+$ T cells were plated into a 96-well, round-bottom plate at a cell density of $1 \times 10^5$ cells per well and cultured overnight in 200 μl of complete RPMI 1640 as described above in the presence of IL-2 (20 IU/ml) with different concentrations of iPAF1C or equivalent volumes of DMSO. The next day, 2.5 μl of concentrated virus stock was added to each well. Cells were cultured in a dark humidified incubator at 37°C and 5% $CO_2$. On days 2 and 5 after infection, 75 μl of each culture was removed and mixed 1:1 with freshly made 2% formaldehyde in PBS (Sigma-Aldrich) and stored at 4°C for analysis by flow cytometry. Cultures were supplemented with 75 ml of complete IL-2–containing RPMI 1640 medium and returned to the incubator.

### J-Lat reactivation assay

J-Lat 5A8, J-Lat 11.1, and J-Lat 6.3 cell lines were plated in 96-well flat bottom plates at a density of 150,000 cells/250 μl supplemented RPMI 1640. Cells were DMSO-treated or treated with iPAF1C (12.5 μM), JQ1 (1 μM), PHA (0.5 μg/ml), and PMA (1 nM) for 48 hours. Cells were then washed in PBS and resuspended in PBS + 1% formaldehyde and fixed for 30 min. Analysis was performed by flow cytometry gating on GFP-positive cells.

### Flow cytometry and analysis of infection data

Flow cytometry analysis was performed on an Attune NxT acoustic focusing cytometer (Thermo Fisher Scientific), recording all events in a 40-μl sample volume after one 150 μl of mixing cycle. Data were exported as FCS3.0 files using Attune NxT Software v3.2.0 and analyzed with a consistent template on FlowJo. Briefly, cells were gated for lymphocytes by light scatter followed by doublet discrimination in both side and forward scatter. Cells with equal fluorescence in the BL-1 (GFP) channel and the VL-2 (AmCyan) channel were identified as autofluorescent and excluded from the analysis. A consistent gate was then used to quantify the fraction of remaining cells that expressed GFP.

### Ex vivo validations of cell-associated viral RNA (vRNA) expression after LRA treatment in HIV-1–infected patients on suppressive antiretroviral therapy

#### *Study subjects*

We selected four study subjects enrolled in the Northwestern University Clinical Research Site for the MWCCS. The four men were well-suppressed patients who had received antiretroviral drugs for at least 5 years. Subject A received stavudine, tenofovir, lamivudine, and nevirapine; subject B received efavirenz, lopinavir, and tenofovir; subject C received ritonavir, amprenavir, and lamivudine/zidovudine; and subject D received indinavir and lamivudine at the sampling visits. We obtained PBMCs from cryostorage more than 5 years after starting antiretroviral therapy and undetectable plasma HIV-1 (<50 copies/ml). Laboratory procedures for clinical sample management are described elsewhere (*82*). The Institutional Review Board of Northwestern University approved the study (STU00022906-CR0008) with most recent approval date of 16 May 2022. All participants provided written informed consent.

#### *Total RNA isolation*

We isolated total RNA from cultured 1 million PBMCs without or treated with LRA (JQ1, PHA, PMA, and iPAF1C) using an RNeasy kit (Qiagen), with the optional on-column deoxyribonuclease I digestion step. The isolated total RNA was eluted in ribonuclease-free water, cleaned, and concentrated using the RNA Clean and Concentration kit (Zymo) and assessed for quality by Qubit (Thermo Fisher Scientific). The final RNA concentration and RNA integrity number were measured using 4200 TapeStation (Agilent) before qRT-PCR.

#### *Validation of cell-associated HIV-1 RNA*

We performed real-time qRT-PCR using an HIV-1-*gag*–specific primers-probe (FAM) set: HIV-1-gagF, 5′-GGTGCGAGAGCGTC AGTATTAAG-3′; HIV-1-gagR, 5′-AGCTCCCTGCTTGCCCATA-3′; HIV-1-gagProbe, 6FAM-5′-TGGGAAAAAATTCGGTTAAGG CCAGGG-3′-QSY. We used the *lactate dehydrogenase A* (*LDHA*) gene for the internal normalization primers-probe (VIC) set (VIC-MGB: assay ID Hs03405707_g1; TaqMan Gene Expression Assay, Thermo Fisher Scientific). Briefly, a 10-μl RT-PCR mixture contained TaqMan Fast Virus 1-Step Master Mix, 400 nM forward and reverse HIV-1-gag primers, 0.3 μl of *LDHA* Gene Expression Assay (Thermo Fisher Scientific), 250 nM each of the TaqMan probes, and 5 μl of extracted RNA or water for the no template controls. We programmed the 7900HT real-time PCR system (Applied Biosystems) for 20 min at 50°C and 20 s at 95°C, followed by 40 cycles of 15 s at 95°C and 60 s at 60°C. The qRT-PCR data were analyzed in technical triplicate. We calculated the fold change in gene expression using the standard ΔΔCT method.

### Statistical analysis

All statistical analyses were performed using GraphPad Prism.

## Supplementary Materials

**This PDF file includes:**

Figs. S1 to S5

View/request a protocol for this paper from *Bio-protocol*.

## REFERENCES AND NOTES


1. F. X. Chen, P. Xie, C. K. Collings, K. Cao, Y. Aoi, S. A. Marshall, E. J. Rendleman, M. Ugarenko, P. A. Ozark, A. Zhang, R. Shiekhattar, E. R. Smith, M. Q. Zhang, A. Shilatifard, PAF1 regulation of promoter-proximal pause release via enhancer activation. *Science* **357**, 1294–1298 (2017).
2. E. Smith, A. Shilatifard, Transcriptional elongation checkpoint control in development and disease. *Genes Dev.* **27**, 1079–1088 (2013).
3. G. Orphanides, T. Lagrange, D. Reinberg, The general transcription factors of RNA polymerase II. *Genes Dev.* **10**, 2657–2683 (1996).
4. B. J. Greber, E. Nogales, The structures of eukaryotic transcription pre-initiation complexes and their functional implications. *Subcell. Biochem.* **93**, 143–192 (2019).
5. B. E. Schwartz, S. Larochelle, B. Suter, J. T. Lis, Cdk7 is required for full activation of Drosophila heat shock genes and RNA polymerase II phosphorylation in vivo. *Mol. Cell. Biol.* **23**, 6876–6886 (2003).
6. K. Adelman, J. T. Lis, Promoter-proximal pausing of RNA polymerase II: Emerging roles in metazoans. *Nat. Rev. Genet.* **13**, 720–731 (2012).
7. L. Core, K. Adelman, Promoter-proximal pausing of RNA polymerase II: A nexus of gene regulation. *Genes Dev.* **33**, 960–982 (2019).
8. M. Noe Gonzalez, D. Blears, J. Q. Svejstrup, Causes and consequences of RNA polymerase II stalling during transcript elongation. *Nat. Rev. Mol. Cell Biol.* **22**, 3–21 (2021).
9. N. F. Marshall, D. H. Price, Purification of P-TEFb, a transcription factor required for the transition into productive elongation. *J. Biol. Chem.* **270**, 12335–12338 (1995).
10. B. M. Peterlin, D. H. Price, Controlling the elongation phase of transcription with P-TEFb. *Mol. Cell* **23**, 297–305 (2006).
11. J. M. Tome, N. D. Tippens, J. T. Lis, Single-molecule nascent RNA sequencing identifies regulatory domain architecture at promoters and enhancers. *Nat. Genet.* **50**, 1533–1541 (2018).
12. C. H. Birkenheuer, J. D. Baines, RNA polymerase II promoter-proximal pausing and release to elongation are key steps regulating herpes simplex virus 1 transcription. *J. Virol.* **94**, e02035-19 (2020).
13. K. Tantale, E. Garcia-Oliver, M.-C. Robert, A. L'Hostis, Y. Yang, N. Tsanov, R. Topno, T. Gostan, A. Kozulic-Pirher, M. Basu-Shrivastava, K. Mukherjee, V. Slaninova, J.-C. Andrau, F. Mueller, E. Basyuk, O. Radulescu, E. Bertrand, Stochastic pausing at latent HIV-1 promoters generates transcriptional bursting. *Nat. Commun.* **12**, 4503 (2021).
14. P. A. Wade, W. Werel, R. C. Fentzke, N. E. Thompson, J. F. Leykam, R. R. Burgess, J. A. Jaehning, Z. F. Burton, A novel collection of accessory factors associated with yeast RNA polymerase II. *Protein Expr. Purif.* **8**, 85–90 (1996).
15. Z. Chen, W. Hankey, Y. Zhao, J. Groth, F. Huang, H. Wang, A. R. Campos, J. Huang, R. G. Roeder, Q. Wang, Transcription recycling assays identify PAF1 as a driver for RNA Pol II recycling. *Nat. Commun.* **12**, 6318 (2021).
16. X. Shi, M. Chang, A. J. Wolf, C. H. Chang, A. A. Frazer-Abel, P. A. Wade, Z. F. Burton, J. A. Jaehning, Cdc73p and Paf1p are found in a novel RNA polymerase II-containing complex distinct from the Srbp-containing holoenzyme. *Mol. Cell. Biol.* **17**, 1160–1169 (1997).
17. Y. Xu, C. Bernecky, C. T. Lee, K. C. Maier, B. Schwalb, D. Tegunov, J. M. Plitzko, H. Urlaub, P. Cramer, Architecture of the RNA polymerase II-Paf1C-TFIIS transcription elongation complex. *Nat. Commun.* **8**, 15741 (2017).
18. B. Zhu, S. S. Mandal, A. D. Pham, Y. Zheng, H. Erdjument-Bromage, S. K. Batra, P. Tempst, D. Reinberg, The human PAF complex coordinates transcription with events downstream of RNA synthesis. *Genes Dev.* **19**, 1668–1673 (2005).
19. F. Chen, B. Liu, L. Guo, X. Ge, W. Feng, D. F. Li, H. Zhou, J. Long, Biochemical insights into Paf1 complex-induced stimulation of Rad6/Bre1-mediated H2B monoubiquitination. *Proc. Natl. Acad. Sci. U.S.A.* **118**, e2025291118 (2021).
20. S. B. Van Oss, M. K. Shirra, A. R. Bataille, A. D. Wier, K. Yen, V. Vinayachandran, I.-J. L. Byeon, C. E. Cucinotta, A. Héroux, J. Jeon, J. Kim, A. P. VanDemark, B. F. Pugh, K. M. Arndt, The histone modification domain of Paf1 complex subunit Rtf1 directly stimulates H2B ubiquitylation through an interaction with Rad6. *Mol. Cell* **64**, 815–825 (2016).
21. A. Wood, J. Schneider, J. Dover, M. Johnston, A. Shilatifard, The Paf1 complex is essential for histone monoubiquitination by the Rad6-Bre1 complex, which signals for histone methylation by COMPASS and Dot1p. *J. Biol. Chem.* **278**, 34739–34742 (2003).
22. A. Wood, N. J. Krogan, J. Dover, J. Schneider, J. Heidt, M. A. Boateng, K. Dean, A. Golshani, Y. Zhang, J. F. Greenblatt, M. Johnston, A. Shilatifard, Bre1, an E3 ubiquitin ligase required for recruitment and substrate selection of Rad6 at a promoter. *Mol. Cell* **11**, 267–274 (2003).
23. A. Wood, J. Schneider, J. Dover, M. Johnston, A. Shilatifard, The Bur1/Bur2 complex is required for histone H2B monoubiquitination by Rad6/Bre1 and histone methylation by COMPASS. *Mol. Cell* **20**, 589–599 (2005).

24. J. Dover, J. Schneider, M. A. Tawiah-Boateng, A. Wood, K. Dean, M. Johnston, A. Shilatifard, Methylation of histone H3 by COMPASS requires ubiquitination of histone H2B by Rad6. *J. Biol. Chem.* **277**, 28368–28371 (2002).
25. X. Chu, X. Qin, H. Xu, L. Li, Z. Wang, F. Li, X. Xie, H. Zhou, Y. Shen, J. Long, Structural insights into Paf1 complex assembly and histone binding. *Nucleic Acids Res.* **41**, 10619–10629 (2013).
26. P. Deng, Y. Zhou, J. Jiang, H. Li, W. Tian, Y. Cao, Y. Qin, J. Kim, R. G. Roeder, D. J. Patel, Z. Wang, Transcriptional elongation factor Paf1 core complex adopts a spirally wrapped solenoidal topology. *Proc. Natl. Acad. Sci. U.S.A.* **115**, 9998–10003 (2018).
27. S. M. Vos, L. Farnung, M. Boehning, C. Wigge, A. Linden, H. Urlaub, P. Cramer, Structure of activated transcription complex Pol II-DSIF-PAF-SPT6. *Nature* **560**, 607–612 (2018).
28. S. M. Vos, L. Farnung, A. Linden, H. Urlaub, P. Cramer, Structure of complete Pol II-DSIF-PAF-SPT6 transcription complex reveals RTF1 allosteric activation. *Nat. Struct. Mol. Biol.* **27**, 668–677 (2020).
29. Y. Xie, M. Zheng, X. Chu, Y. Chen, H. Xu, J. Wang, H. Zhou, J. Long, Paf1 and Ctr9 subcomplex formation is essential for Paf1 complex assembly and functional regulation. *Nat. Commun.* **9**, 3795 (2018).
30. X. Shi, A. Finkelstein, A. J. Wolf, P. A. Wade, Z. F. Burton, J. A. Jaehning, Paf1p, an RNA polymerase II-associated factor in Saccharomyces cerevisiae, may have both positive and negative roles in transcription. *Mol. Cell. Biol.* **16**, 669–676 (1996).
31. L. Hou, Y. Wang, Y. Liu, N. Zhang, I. Shamovsky, E. Nudler, B. Tian, B. D. Dynlacht, Paf1C regulates RNA polymerase II progression by modulating elongation rate. *Proc. Natl. Acad. Sci. U.S.A.* **116**, 14583–14592 (2019).
32. F. X. Chen, A. R. Woodfin, A. Gardini, R. A. Rickels, S. A. Marshall, E. R. Smith, R. Shiekhattar, A. Shilatifard, PAF1, a molecular regulator of promoter-proximal pausing by RNA polymerase II. *Cell* **162**, 1003–1015 (2015).
33. X. Bai, J. Kim, Z. Yang, M. J. Jurynec, T. E. Akie, J. Lee, J. LeBlanc, A. Sessa, H. Jiang, A. DiBiase, Y. Zhou, D. J. Grunwald, S. Lin, A. B. Cantor, S. H. Orkin, L. I. Zon, TIF1γ controls erythroid cell fate by regulating transcription elongation. *Cell* **142**, 133–143 (2010).
34. Y. Aoi, A. P. Shah, S. Ganesan, S. H. A. Soliman, B.-K. Cho, Y. A. Goo, N. L. Kelleher, A. Shilatifard, SPT6 functions in transcriptional pause/release via PAF1C recruitment. *Mol. Cell* **82**, 3412–3423.e5 (2022).
35. L. A. Jaenicke, B. von Eyss, A. Carstensen, E. Wolf, W. Xu, A. K. Greifenberg, M. Geyer, M. Eilers, N. Popov, Ubiquitin-dependent turnover of MYC antagonizes MYC/PAF1C complex accumulation to drive transcriptional elongation. *Mol. Cell* **61**, 54–67 (2016).
36. J. Gu, N. D. Babayeva, Y. Suwa, A. G. Baranovskiy, D. H. Price, T. H. Tahirov, Crystal structure of HIV-1 Tat complexed with human P-TEFb and AFF4. *Cell Cycle* **13**, 1788–1797 (2014).
37. U. Mbonye, B. Wang, G. Gokulrangan, W. Shi, S. Yang, J. Karn, Cyclin-dependent kinase 7 (CDK7)-mediated phosphorylation of the CDK9 activation loop promotes P-TEFb assembly with Tat and proviral HIV reactivation. *J. Biol. Chem.* **293**, 10009–10025 (2018).
38. S. C. Sedore, S. A. Byers, S. Biglione, J. P. Price, W. J. Maury, D. H. Price, Manipulation of P-TEFb control machinery by HIV: Recruitment of P-TEFb from the large form by Tat and binding of HEXIM1 to TAR. *Nucleic Acids Res.* **35**, 4347–4358 (2007).
39. R. Gao, J. Bao, H. Yan, L. Xie, W. Qin, H. Ning, S. Huang, J. Cheng, R. Zhi, Z. Li, B. Tucker, Y. Chen, K. Zhang, X. Wu, Z. Liu, X. Gao, D. Hu, Competition between PAF1 and MLL1/COMPASS confers the opposing function of LEDGF/p75 in HIV latency and proviral reactivation. *Sci. Adv.* **6**, eaaz8411 (2020).
40. S. Castro-Gonzalez, M. Colomer-Lluch, R. Serra-Moreno, Barriers for HIV cure: The latent reservoir. *AIDS Res. Hum. Retroviruses* **34**, 739–759 (2018).
41. J. Grau-Expósito, L. Luque-Ballesteros, J. Navarro, A. Curran, J. Burgos, E. Ribera, A. Torrella, B. Planas, R. Badía, M. Martin-Castillo, J. Fernández-Sojo, M. Genescà, V. Falcó, M. J. Buzon, Latency reversal agents affect differently the latent reservoir present in distinct CD4+ T subpopulations. *PLOS Pathog.* **15**, e1007991 (2019).
42. A. Timmons, E. Fray, M. Kumar, F. Wu, W. Dai, C. K. Bullen, P. Kim, C. Hetzel, C. Yang, S. Beg, J. Lai, J. L. Pomerantz, S. A. Yukl, J. D. Siliciano, R. F. Siliciano, HSF1 inhibition attenuates HIV-1 latency reversal mediated by several candidate LRAs in vitro and ex vivo. *Proc. Natl. Acad. Sci. U.S.A.* **117**, 15763–15771 (2020).
43. Y.-C. Ho, L. Shan, N. N. Hosmane, J. Wang, S. B. Laskey, D. I. S. Rosenbloom, J. Lai, J. N. Blankson, J. D. Siliciano, R. F. Siliciano, Replication-competent noninduced proviruses in the latent reservoir increase barrier to HIV-1 cure. *Cell* **155**, 540–551 (2013).
44. S. R. Jefferys, S. D. Burgos, J. J. Peterson, S. R. Selitsky, A.-M. W. Turner, L. I. James, Y.-H. Tsai, A. R. Coffey, D. M. Margolis, J. Parker, E. P. Browne, Epigenomic characterization of latent HIV infection identifies latency regulating transcription factors. *PLOS Pathog.* **17**, e1009346 (2021).
45. Y. Kim, J. L. Anderson, S. R. Lewin, Getting the "kill" into "shock and kill": Strategies to eliminate latent HIV. *Cell Host Microbe* **23**, 14–26 (2018).
46. V. E. Walker-Sperling, C. W. Pohlmeyer, P. M. Tarwater, J. N. Blankson, The effect of latency reversal agents on primary CD8+ T cells: Implications for shock and kill strategies for human immunodeficiency virus eradication. *EBioMedicine* **8**, 217–229 (2016).
47. E. Abner, M. Stoszko, L. Zeng, H. C. Chen, A. Izquierdo-Bouldstridge, T. Konuma, E. Zorita, E. Fanunza, Q. Zhang, T. Mahmoudi, M. M. Zhou, G. J. Filion, A. Jordan, A new quinoline BRD4 inhibitor targets a distinct latent HIV-1 reservoir for reactivation from other "shock" drugs. *J. Virol.* **92**, e02056-17 (2018).
48. A. Blanco, T. Mahajan, R. A. Coronado, K. Ma, D. R. Demma, R. D. Dar, Synergistic chromatin-modifying treatments reactivate latent HIV and decrease migration of multiple host-cell types. *Viruses* **13**, 1097 (2021).
49. R. Fromentin, S. DaFonseca, C. T. Costiniuk, M. El-Far, F. A. Procopio, F. M. Hecht, R. Hoh, S. G. Deeks, D. J. Hazuda, S. R. Lewin, J.-P. Routy, R.-P. Sékaly, N. Chomont, PD-1 blockade potentiates HIV latency reversal ex vivo in CD4(+) T cells from ART-suppressed individuals. *Nat. Commun.* **10**, 814 (2019).
50. J. L. Sloane, N. L. Benner, K. N. Keenan, X. Zang, M. S. A. Soliman, X. Wu, M. Dimapasoc, T. W. Chun, M. D. Marsden, J. A. Zack, P. A. Wender, Prodrugs of PKC modulators show enhanced HIV latency reversal and an expanded therapeutic window. *Proc. Natl. Acad. Sci. U.S.A.* **117**, 10688–10698 (2020).
51. A. Ait-Ammar, A. Kula, G. Darcis, R. Verdikt, S. De Wit, V. Gautier, P. W. G. Mallon, A. Marcello, O. Rohr, C. Van Lint, Current status of latency reversing agents facing the heterogeneity of HIV-1 cellular and tissue reservoirs. *Front. Microbiol.* **10**, 3060 (2019).
52. J. J. Irwin, B. K. Shoichet, ZINC—A free database of commercially available compounds for virtual screening. *J. Chem. Inf. Model.* **45**, 177–182 (2005).
53. D. Martinez Molina, R. Jafari, M. Ignatushchenko, T. Seki, E. A. Larsson, C. Dan, L. Sreekumar, Y. Cao, P. Nordlund, Monitoring drug target engagement in cells and tissues using the cellular thermal shift assay. *Science* **341**, 84–87 (2013).
54. D. B. Mahat, H. H. Salamanca, F. M. Duarte, C. G. Danko, J. T. Lis, Mammalian heat shock response and mechanisms underlying its genome-wide transcriptional regulation. *Mol. Cell* **62**, 63–78 (2016).
55. A. Vihervaara, D. B. Mahat, M. J. Guertin, T. Chu, C. G. Danko, J. T. Lis, L. Sistonen, Transcriptional response to stress is pre-wired by promoter and enhancer architecture. *Nat. Commun.* **8**, 255 (2017).
56. D. C. Cary, K. Fujinaga, B. M. Peterlin, Molecular mechanisms of HIV latency. *J. Clin. Invest.* **126**, 448–454 (2016).
57. Z. Li, J. Guo, Y. Wu, Q. Zhou, The BET bromodomain inhibitor JQ1 activates HIV latency through antagonizing Brd4 inhibition of Tat-transactivation. *Nucleic Acids Res.* **41**, 277–287 (2013).
58. S. A. Yukl, P. Kaiser, P. Kim, S. Telwatte, S. K. Joshi, M. Vu, H. Lampiris, J. K. Wong, HIV latency in isolated patient $CD4^+$ T cells may be due to blocks in HIV transcriptional elongation, completion, and splicing. *Sci. Transl. Med.* **10**, eaap9927 (2018).
59. Z. Wang, A. Song, H. Xu, S. Hu, B. Tao, L. Peng, J. Wang, J. Li, J. Yu, L. Wang, Z. Li, X. Chen, M. Wang, Y. Chi, J. Wu, Y. Xu, H. Zheng, F. X. Chen, Coordinated regulation of RNA polymerase II pausing and elongation progression by PAF1. *Sci. Adv.* **8**, eabm5504 (2022).
60. J. Kim, M. Guermah, R. K. McGinty, J. S. Lee, Z. Tang, T. A. Milne, A. Shilatifard, T. W. Muir, R. G. Roeder, RAD6-mediated transcription-coupled H2B ubiquitylation directly stimulates H3K4 methylation in human cells. *Cell* **137**, 459–471 (2009).
61. N. J. Krogan, J. Dover, A. Wood, J. Schneider, J. Heidt, M. A. Boateng, K. Dean, O. W. Ryan, A. Golshani, M. Johnston, J. F. Greenblatt, A. Shilatifard, The Paf1 complex is required for histone H3 methylation by COMPASS and Dot1p: Linking transcriptional elongation to histone methylation. *Mol. Cell* **11**, 721–729 (2003).
62. A. Strikoudis, C. Lazaris, P. Ntziachristos, A. Tsirigos, I. Aifantis, Opposing functions of H2BK120 ubiquitylation and H3K79 methylation in the regulation of pluripotency by the Paf1 complex. *Cell Cycle* **16**, 2315–2322 (2017).
63. K. Tenney, M. Gerber, A. Ilvarsonn, J. Schneider, M. Gause, D. Dorsett, J. C. Eissenberg, A. Shilatifard, *Drosophila* Rtf1 functions in histone methylation, gene expression, and *Notch* signaling. *Proc. Natl. Acad. Sci. U.S.A.* **103**, 11970–11974 (2006).
64. S. Cugusi, R. Mitter, G. P. Kelly, J. Walker, Z. Han, P. Pisano, M. Wierer, A. Stewart, J. Q. Svejstrup, Heat shock induces premature transcript termination and reconfigures the human transcriptome. *Mol. Cell* **82**, 1573–1588.e10 (2022).
65. D. Boehm, V. Calvanese, R. D. Dar, S. Xing, S. Schroeder, L. Martins, K. Aull, P.-C. Li, V. Planelles, J. E. Bradner, M.-M. Zhou, R. F. Siliciano, L. Weinberger, E. Verdin, M. Ott, BET bromodomain-targeting compounds reactivate HIV from latency via a Tat-independent mechanism. *Cell Cycle* **12**, 452–462 (2013).
66. K. Chaudhary, S. Deb, N. Moniaux, M. P. Ponnusamy, S. K. Batra, Human RNA polymerase II-associated factor complex: Dysregulation in cancer. *Oncogene* **26**, 7499–7507 (2007).
67. M. E. Massett, L. Monaghan, S. Patterson, N. Mannion, R. P. Bunschoten, A. Hoose, S. Marmiroli, R. M. J. Liskamp, H. G. Jørgensen, D. Vetrie, A. M. Michie, X. Huang, A KDM4A-PAF1-mediated epigenomic network is essential for acute myeloid leukemia cell self-renewal and survival. *Cell Death Dis.* **12**, 573 (2021).
68. A. G. Muntean, J. Tan, K. Sitwala, Y. Huang, J. Bronstein, J. A. Connelly, V. Basrur, K. S. J. Elenitoba-Johnson, J. L. Hess, The PAF complex synergizes with MLL fusion proteins at *HOX* loci to promote leukemogenesis. *Cancer Cell* **17**, 609–621 (2010).

69. N. Saha, J. Ropa, L. Chen, H. Hu, M. Mysliwski, A. Friedman, I. Maillard, A. G. Muntean, The PAF1c subunit CDC73 is required for mouse hematopoietic stem cell maintenance but displays leukemia-specific gene regulation. *Stem Cell Rep.* **12**, 1069–1083 (2019).
70. B. Zhang, Z.-y. Liu, R. Wu, C.-m. Zhang, K. Cao, W.-g. Shan, Z. Liu, M. Ji, Z.-l. Tian, G. Sethi, H.-l. Shi, R.-h. Wang, Transcriptional regulator CTR9 promotes hepatocellular carcinoma progression and metastasis via increasing PEG10 transcriptional activity. *Acta Pharmacol. Sin.* **43**, 2109–2118 (2022).
71. J. B. Baell, G. A. Holloway, New substructure filters for removal of pan assay interference compounds (PAINS) from screening libraries and for their exclusion in bioassays. *J. Med. Chem.* **53**, 2719–2740 (2010).
72. T. I. Lee, S. E. Johnstone, R. A. Young, Chromatin immunoprecipitation and microarray-based analysis of protein location. *Nat. Protoc.* **1**, 729–748 (2006).
73. E. Bartom, in CETO Toolbox (github.com, 2018), vol. 2022, pp. CETO Toolbox.
74. A. M. Bolger, M. Lohse, B. Usadel, Trimmomatic: A flexible trimmer for Illumina sequence data. *Bioinformatics* **30**, 2114–2120 (2014).
75. B. Langmead, S. L. Salzberg, Fast gapped-read alignment with Bowtie 2. *Nat. Methods* **9**, 357–359 (2012).
76. B. Langmead, C. Trapnell, M. Pop, S. L. Salzberg, Ultrafast and memory-efficient alignment of short DNA sequences to the human genome. *Genome Biol.* **10**, R25 (2009).
77. D. Kim, G. Pertea, C. Trapnell, H. Pimentel, R. Kelley, S. L. Salzberg, TopHat2: Accurate alignment of transcriptomes in the presence of insertions, deletions and gene fusions. *Genome Biol.* **14**, R36 (2013).
78. S. Anders, P. T. Pyl, W. Huber, HTSeq—A Python framework to work with high-throughput sequencing data. *Bioinformatics* **31**, 166–169 (2015).
79. D. Risso, J. Ngai, T. P. Speed, S. Dudoit, Normalization of RNA-seq data using factor analysis of control genes or samples. *Nat. Biotechnol.* **32**, 896–902 (2014).
80. D. B. Mahat, H. Kwak, G. T. Booth, I. H. Jonkers, C. G. Danko, R. K. Patel, C. T. Waters, K. Munson, L. J. Core, J. T. Lis, Base-pair-resolution genome-wide mapping of active RNA polymerases using precision nuclear run-on (PRO-seq). *Nat. Protoc.* **11**, 1455–1476 (2016).
81. A. R. Quinlan, I. M. Hall, BEDTools: A flexible suite of utilities for comparing genomic features. *Bioinformatics* **26**, 841–842 (2010).
82. R. Detels, L. Jacobson, J. Margolick, O. Martinez-Maza, A. Muñoz, J. Phair, C. Rinaldo, S. Wolinsky, The multicenter AIDS cohort study, 1983 to .... *Public Health* **126**, 196–198 (2012).

**Acknowledgments:** We thank S. Gold, M. A. Morgan, and B. K. Cenik for reading the manuscript and providing critical feedback. We also thank the Shilatifard and Hultquist present and past laboratory members for discussions during this work; B. Monroe for illustrations; and N. H. Khan, A. P. Shah, and E. Rendleman for initial NGS support. **Funding:** This research was supported by NIH/NIAID funding for the HIV-1 Accessory & Regulatory Complexes (HARC) Center (P50 AI150476 to J.F.H.), NIH/NIAID funding for the Third Coast Center for AIDS Research (P30 AI117943 to J.F.H.), and several NIH/NIAID grants for HIV-1 research (R01 AI150455, R01 AI165236, and R01 AI150998 to J.F.H.). The study was also supported by funding from NIH/NHLBI grant U01HL146240 to S.M.W. and National Cancer Institute grant R35CA197569 to A.S.
**Author contributions:** S.H.A.S. and A.S. conceived and designed the experiments to generate PAF1C inhibitors; S.H.A.S. performed the screening and transcriptional profiling experiments to identify and characterize PAF1C inhibitors; S.H.A.S., A.S., J.F.H., W.J.C. discussed the relevance of iPAF1C in HIV-1 reversal and designed appropriate studies; S.H.A.S. performed the transcriptional studies in HIV-1 latency models; W.J.C. performed the HIV-1 experiments and contributed to manuscript and writing the relevant portion of the paper; W.J.C., E.-Y.K., M.W., J.F.H., and S.M.W. performed latency reversal assays in patient cells; M.I. analyzed NGS data; Y.A. repeated RNA-seq data; S.G. and J.M.Z. performed NGS; R.K.M. performed structure-based drug screen; S.H.A.S., W.J.C., J.F.H., and A.S. interpreted the results and wrote the manuscript, with input from all authors. **Competing interests:** The authors declare that they have no competing interests. **Data and materials availability:** All data needed to evaluate the conclusions in the paper are present in the paper and/or the Supplementary Materials. All NGS data are deposited under GEO accession: GSE211651.

Submitted 8 October 2022
Accepted 3 February 2023
Published 8 March 2023
10.1126/sciadv.adf2468